Nanocrystallites Modulate Intermolecular Interactions in Cryoprotected Protein Solutions

Mariia Filianina,* Maddalena Bin, Sharon Berkowicz, Mario Reiser, Hailong Li, Sonja Timmermann, Malte Blankenburg, Katrin Amann-Winkel, Christian Gutt, and Fivos Perakis*

ACCESS | Metrics & More | Article Recommendations | SI Supporting Information

ABSTRACT: Studying protein interactions at low temperatures has important implications for optimizing cryostorage processes of biological tissue, food, and protein-based drugs. One of the major issues is related to the formation of ice nanocrystals, which can occur even in the presence of cryoprotectants and can lead to protein denaturation. The presence of ice nanocrystals in protein solutions poses several challenges since, contrary to microscopic ice crystals, they can be difficult to resolve and can complicate the interpretation of experimental data. Here, using a combination of small- and wide-angle X-ray scattering (SAXS and WAXS), we investigate the structural evolution of concentrated lysozyme solutions in a cryoprotected glycerol−water mixture from room temperature (T = 300 K) down to cryogenic temperatures (T = 195 K). Upon cooling, we observe a transition near the melting temperature of the solution ($T \approx$ 245 K), which manifests both in the temperature dependence of the scattering intensity peak position reflecting protein−protein length scales (SAXS) and the interatomic distances within the solvent (WAXS). Upon thermal cycling, a hysteresis is observed in the scattering intensity, which is attributed to the formation of nanocrystallites in the order of 10 nm. The experimental data are well described by the two-Yukawa model, which indicates temperature-dependent changes in the short-range attraction of the protein−protein interaction potential. Our results demonstrate that the nanocrystal growth yields effectively stronger protein−protein attraction and influences the protein pair distribution function beyond the first coordination shell.
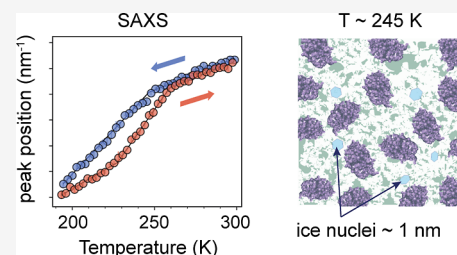
INTRODUCTION

Organisms that thrive in cold environments have evolved unique strategies to enable survival, including the accumulation of osmolytes and the usage of specialized cryoprotectants.[1] However, protein functionality at low temperatures remains poorly understood due to experimental challenges related to ice formation, which limits the investigation of biomolecules in deeply supercooled environments. Understanding the effect of cryoprotectants in low-temperature protein solutions is important for elucidating the combined effect of the solutes on the freezing point depression and has significant implications for biotechnical cryostorage applications.[2]

At low temperatures and below what is known as the protein dynamic transition ($T_d \approx$ 230 K), proteins are believed to lose their conformational flexibility required for biological function.[3,4] Although the origin of this effect is still debated, it has been reported for many biopolymers and is now accepted as a generic feature of hydrated proteins, while it is absent in dehydrated systems.[5,6] Experimental studies suggest that this effect stems from the crossover in proteins' intrinsic dynamics from harmonic to anharmonic motions above T_d[3] and that temperature-induced phenomena in the hydration shell and the bulk solvent play a crucial role.[7−14] An important observation is that the transition temperature, observed in the mean square displacement amplitude, depends on the

properties and the amount of the molecules surrounding the protein surface.[8,9] Such sensitivity of biomolecules to the solvent implies the possibility to control both the onset and the amplitude of the protein anharmonic motions related to the dynamical transition by choosing a suitable environment,[8,10] which can have various practical consequences in connection with the development of biological cryogenic techniques.[2]

This aspect further emphasizes the importance to accurately account for the critical phenomena in the solvent itself. For example, glycerol is widely employed in studies of low-temperature protein dynamics[15−19] and structure[20] due to its ability to induce strong frustration against water crystallization.[21,22] This effect arises from the observation that the glycerol molecules affect the local structure and hydrogen bonding of water[18,23] and suppress the tetrahedral component.[24] Furthermore, glycerol aqueous solutions have been hypothesized to exhibit a liquid−liquid transition,[22,25] although the physical understanding for this phenomenon is still

debated. Early experimental studies ascribe the observed low-temperature transition in glycerol−water mixtures to the genuine liquid−liquid transition,[22,25] whereas follow-up investigations suggest that the observed transition may be due to nanocrystallite formation, which occurs due to the demixing of glycerol−water mixtures at lower temperatures.[60] Importantly, these effects in glycerol can be experimentally observed in a narrow range of the glycerol concentration from 15 to 28 mol %,[26−29] which is close to those typically used in cryopreservation applications for biological molecules, cells, and embryos.[2,30] Hence, a unified understanding of the mutual effects of the solvent on the proteins and vice versa at low temperature remains of fundamental importance.

Here, we focus on the structural investigation of cryoprotected protein solutions in a wide temperature range. Using small- and wide-angle X-ray scattering (SAXS/WAXS), we study lysozyme in glycerol−water solutions (23 mol % glycerol). The combination of SAXS/WAXS allows us to simultaneously follow the changes in the intermolecular protein−protein and interatomic interactions within the solvent. Measurements are performed over a broad range of temperatures including thermal cycles cooling from room temperature ($T = 300$ K) down to $T = 195$ K and warming back up. We model the measured SAXS intensities with the two-Yukawa potential describing the protein−protein interactions to elucidate the origin of the observed temperature-induced transitions.

◼ METHODS

Materials and Sample Preparation. For the cryoprotective solvent, glycerol (49770, purchased from Honeywell) was mixed with MilliQ water to obtain a glycerol concentration of 23 mol % (corresponding to 55 vol % or 60 wt %). Lysozyme from hen egg white (14.3 kDa) was purchased from Sigma-Aldrich (L6876) and was used without further purification. The protein powder was dissolved in the 23 mol % glycerol−water solution with protein concentrations of 10 and 200 mg/mL. The resulting pH of the protein solutions was measured to be 4.1 ± 0.1 at room temperature, similar to the pH range used in previous studies of lysozyme in glycerol−water mixtures.[31−34] Since lysozyme is known to exhibit a maximum thermal stability at pH $\approx$ 5, while high pH values promote the aggregation of unfolded lysozyme,[35,36] no additional salt was added to the system. The resulting solutions were filled in quartz capillaries of 1.5 mm in diameter for X-ray scattering studies.

Experimental X-ray Parameters. SAXS and WAXS experiments were carried out at the high-energy X-ray diffraction beamline P21.1 at PETRA III (DESY, Hamburg), using the experimental parameters as detailed in Table 1. The measured two-dimensional (2D) X-ray scattering patterns were azimuthally averaged to obtain the $I(Q)$ curves. The resulting scattering curves were corrected for solvent and background scattering by subtracting the scattering intensity measured on a capillary filled with a glycerol−water solvent of the same concentration. A Linkam scientific instruments stage (model HFSX350) was used to control and vary the sample temperature within a broad range from $T = 300$ K to $T = 195$ K. For all measurements, the temperature was varied with the rate of 4 K/min and the SAXS/WAXS scattering patterns were measured simultaneously and continuously as the temperature was varied (see the Supporting Information). Measurements of the temperature cycles were performed on

Table 1. Experimental X-ray Parameters Used for the Experiment, Including the Photon Energy, Beam Size, Flux, Sample Environment, Detector, and Sample-Detector Distance (SDD) for SAXS and WAXS Geometries

photon energy (keV)	52.5
beam size (μm^2)	500×500
flux ($\times 10^9$ ph/s)	12.5
sample environment	Linkam stage
SAXS detector	Pilatus3 X CdTe 2M
SAXS SDD (m)	14.6
WAXS detector	Varex XRD4343CT
WAXS SDD (m)	1.0

different capillaries filled with identical samples of the same solution. Each temperature cycle was measured on a single spot of the sample.

Data Analysis and Modeling. The scattering patterns acquired with the 2D detectors were normalized by the intensity of the transmitted beam, azimuthally averaged using the pyFAI python library[37] followed by the subtraction of the solvent scattering.

The scattering intensity $I(Q)$ as a function of the momentum transfer $Q = \frac{4\pi}{\lambda}\sin\theta$, where 2θ is the scattering angle and λ is the wavelength of the X-ray radiation, was modeled by the following expression

$$I(Q) = \phi V \Delta\rho^2 \langle P(Q) \rangle S(Q) + c \tag{1}$$

Here, $\Delta\rho$ is the averaged contrast term, and V and ϕ are the volume and the volume fraction of an individual protein, respectively. The orientation-averaged form factor $\langle P(Q) \rangle$ is related to the protein size and structure, while the structure factor $S(Q)$ provides information about the protein−protein interactions, which for dilute solutions of non-interacting proteins corresponds to $S(Q) \approx 1$. c is the background offset, which was determined based on the large Q asymptotic value at about $Q \approx 3.5$ nm^{-1}. The volume fraction is $\phi \approx 0.15$ for the 200 mg/mL lysozyme solution and was used as a fixed parameter for the data analysis.

For lysozyme in solution, the form factor can be described by that of an ellipsoid of revolution[38−40] as

$$P(Q) = \int_0^1 \frac{j_1(Q\sqrt{r_a^2 + x^2(r_b^2 - r_a^2)})^2}{(Q\sqrt{r_a^2 + x^2(r_b^2 - r_a^2)})^4} dx \tag{2}$$

where r_a and r_b are the ellipsoid semi axes. In this work, the experimental $I(Q)$ curves for the lowest protein concentration were fitted with a normalized radially averaged scattering function of an ellipsoid with a fixed aspect ratio of $r_a/r_b = 1.5$[38,41] calculated with Jscatter,[42] while keeping the major semi axis as a fitting parameter.

The $S(Q)$ is related to the effective interaction potential $U(r)$ through the direct correlation function, which in turn can be obtained within the mean spherical approximation.[39,41] Here, we use the two-Yukawa (TY) potential to describe the protein−protein interaction, which has been previously used successfully to describe the lysozyme structure factor at highly concentrated conditions.[38,41,43] The TY potential comprises a short-range attraction and a long-range repulsion term as follows

$$\frac{U(r)}{k_{\mathrm{B}}T} = \begin{cases} \infty, & \text{where } r < \sigma \\ -K_1\frac{e^{-Z_1(r/\sigma-1)}}{r/\sigma} + K_2\frac{e^{-Z_2(r/\sigma-1)}}{r/\sigma}, & \text{where } r \geq \sigma \end{cases}$$

$$(3)$$

Here, k_{B} is the Boltzmann constant, T is the temperature, r is the protein−protein distance, and σ is the effective diameter. Moreover, Z_1 and Z_2 determine the range of the attractive and repulsive Yukawa potential terms in units of σ, respectively, while K_1 and K_2 correspond to the attractive and repulsive interaction strength in units of $k_{\mathrm{B}}T$.

In the modeling of interactions, the attraction strength K_1 is used as a fitting parameter, while the parameters $Z_1 = 21$, $K_2 = 3.2$, and $Z_2 = 3.5$ are fixed.[38] The shape parameters, such as the particle diameter, which in terms of the ellipsoid parameters is $\sigma = 2(r_a r_b^2)^{1/3}$, were obtained independently from the form factor analysis.

RESULTS AND DISCUSSION

Figure 1 shows the variation of the SAXS scattering intensity measured for a dilute (panel A, 10 mg/mL) and concentrated
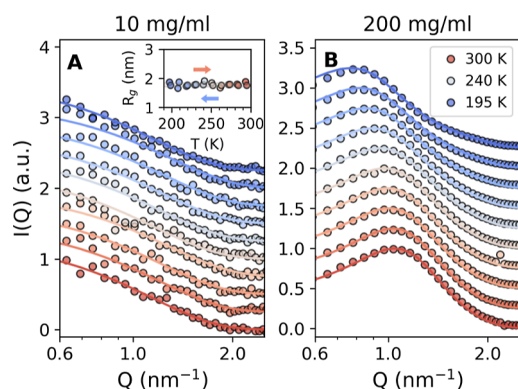

Figure 1. SAXS intensities of 10 mg/mL (panel A) and 200 mg/mL (panel B) lysozyme in 23 mol % glycerol−water solution as a function of temperature while cooling down from room temperature, $T = 300$ K (red) to $T = 195$ K (blue). Here, an offset has been added to facilitate the comparison. The symbols represent the experimental data, while the solid lines are the fits from the model. The inset (panel A) shows the radius of gyration R_{g} as a function of temperature as extracted from the fits in panel A during cooling and heating.

(panel B, 200 mg/mL) lysozyme glycerol−water solution upon cooling the sample from room temperature ($T = 300$ K) down to $T = 195$ K. The scattering patterns were recorded continuously during the temperature sweep with a cooling rate of 4 K/min, and here we show the $I(Q)$ curves averaged over the temperature interval of ≈ 10 K.

As seen in Figure 1A, the scattering patterns at the lowest protein concentration (10 mg/mL) exhibit negligible interference effects and are adequately fitted with the computed scattering intensity of an ellipsoid of revolution with a fixed aspect ratio of $r_a/r_b = 1.5$. The resulting fits to the data are shown as solid lines in Figure 1A for various temperatures. As shown in the inset in Figure 1A, no significant variation is observed in the radius of gyration R_{g} in the entire temperature range, suggesting that we do not observe any significant changes in the protein size related to cold denaturation.[44,45] For all temperatures, the gyration radii are determined to be $R_{\mathrm{g}} = 1.78 \pm 0.07$ nm, which reasonably agrees with the

literature values for lysozyme.[38,46] In the presence of glycerol, lysozyme is known to slightly compactify[33] while still remaining in its quasi-native state.[47]

We can attribute the absence of major structural changes at low temperatures to the stabilizing action of glycerol. While water has been shown to be a key player in cold denaturation[48,49] which occurs for many proteins at 210−250 K, the addition of an organic co-solvent has been shown to dramatically attenuate low-temperature unfolding.[49,50] Furthermore, since many of the structural effects of organic solvents on proteins are due to the dielectric constant,[51] the combination of low temperature and high glycerol concentration is in fact advantageous, as it brings the dielectric constant value close to ambient conditions in water.[52,53]

Additional stabilizing influences include the high enthalpy of activation for protein denaturation[51,54] and preferential exclusion[55,56] from specific patches on the protein surface, both of which will contribute toward the preservation of the native form at low temperatures. A more comprehensive discussion of the effects of subzero temperatures and organic solvents on the protein structure is presented elsewhere.[57]

The scattering patterns for higher protein concentration (200 mg/mL) shown in Figure 1B exhibit an interference peak close to $Q \approx 1$ nm^{-1} at room temperature, related to the intermolecular protein structure factor. With decreasing temperature, the peak shifts to lower Q values in the entire temperature range accessed here. This behavior is consistent with the temperature trends reported for lysozyme in buffer solutions under ambient conditions in previous studies.[38,40,58] The solid lines represent the fits of the $I(Q)$ curves using the TY model in order to extract the structure factor, as described in the Methods section. The calculated structure factor $S(Q)$ using the best fit parameters is shown in Figure 4A, and the temperature dependence of the fit parameter is shown in Figure 4B, which are discussed in the following paragraphs.

Figure 2 shows the variation of the WAXS scattering intensities of the 200 mg/mL lysozyme glycerol−water solution upon cooling down to 195 K (panel A) and warming back to room temperature (panel B). The insets in both panels represent the data in contour plots zoomed in around the first peak in the $I(Q)$ where the ice signal is expected. The peaks in this Q-range are known to arise from scattering on interatomic length scales.

One can see that upon cooling, the Q position of the first peak located at $Q_{\mathrm{m}}^{\mathrm{WAXS}} \approx 16.4$ nm^{-1} at room temperature shifts to higher values and the peak shape narrows. The temperature trend observed for the glycerol−water mixture with the given glycerol concentration is opposite of what is known for pure water.[59] In other words, while the Q spacing between the first and the second peaks in water is known to increase with decreasing temperature, Figure 2 shows that both peaks move together to higher Q values. We also note that even at the lowest temperatures (195 K), there are no detectable ice peaks, indicating that the system is not in its crystalline state even at such low temperatures thanks to the presence of glycerol.

Upon heating, however, ice peaks start to be discernible in the WAXS intensities, as seen in Figure 2B. Here, the black arrows indicate the Q positions of several ice I_{h} Bragg peaks. The 2D scattering patterns recorded by the detector at $T = 197$ and 245 K are presented in panels C and D, respectively. One can see several sporadic ice Bragg peaks at 197 K, which are already absent at 245 K.
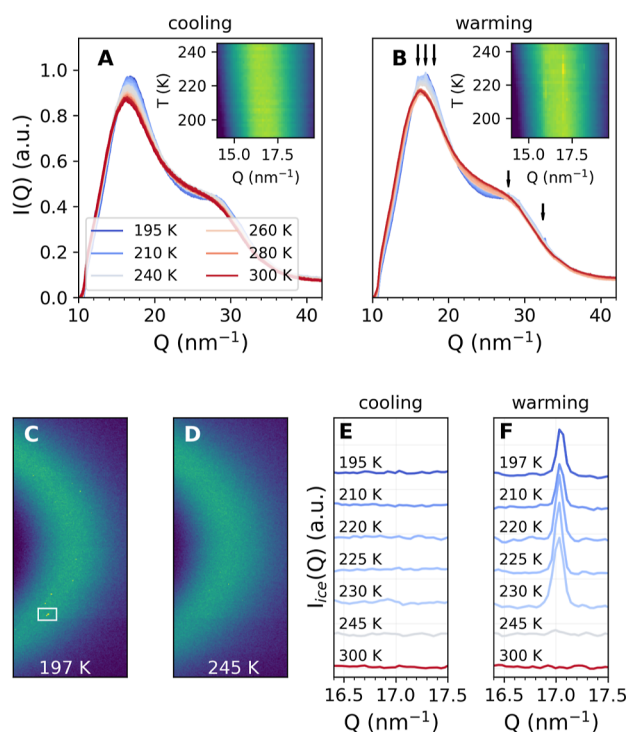
Figure 2. WAXS of a 200 mg/mL lysozyme in 23 mol % glycerol–water solution as a function of temperature while cooling down from $T = 300$ K to $T = 195$ K (panel A) and warming back up to room temperature (panel B). The insets in both panels represent the data in contour plots to emphasize that the ice peaks are absent during the cooldown and manifest during the warm-up. The black arrows in panel B indicate the peaks matching some of the Bragg peaks of hexagonal ice. (C,D) representative 2D scattering patterns measured upon heating at $T = 197$ K and $T = 245$ K, where ice peaks appear in the former case. The white rectangle (panel C) highlights the ice peak whose profile along the radial direction is plotted in panels E and F upon cooling and warming, respectively. In panels E and F, an offset has been added to facilitate the comparison between temperatures.

For further analysis, we focus on one of the ice Bragg peaks highlighted in Figure 2C by a white rectangle and follow its evolution at different temperatures during cooling and heating. This peak corresponds to the ice I_h [002] diffraction peak centered at ≈ 17 nm^{-1} in the $I(Q)$ curves shown in panel B. We calculate the contribution from the ice peak by subtracting the diffuse part of the WAXS scattering. The resulting ice peak intensities I_{ice} as a function of the momentum transfer Q (i.e., radial direction of the 2D scattering patterns) are shown in Figure 2F during heating. We note that this ice peak is absent during the cooling down until 195 K (Figure 2E).

One can see that the ice peak starts to develop already at $T \approx 197$ K and disappears at $T \approx 245$ K, which is slightly above the expected melting temperature for the 23 mol % glycerol–water mixture.[25,60] From the width of the ice peak, we can estimate the ice crystallite size based on Scherrer's equation,[61,62] $\delta = \frac{\lambda}{\beta \cos \theta}$, where δ is the apparent crystallite's size, λ is the wavelength, and β is the breadth of the Bragg peak at scattering angle θ. In this case, β is calculated as the integral area beneath the peak divided by its maximum amplitude. Using this approach, we estimate that the ice crystallites starting from 197 K are $\approx 12-15$ nm in size. Furthermore, the formation of ice nanocrystals of comparable sizes upon heating is also observed in the pure glycerol–water mixture as well as

in the 10 mg/mL lysozyme in glycerol–water solution as discussed in the Supporting Information. From the observed increase of the Bragg peak intensities during the warm-up, the number density of these nanocrystallites also increases until $T \approx 240-245$ K after which no ice peaks are visible anymore. The formation of ice nanocrystallites upon heating is attributed, for pure glycerol–water mixture of similar concentrations, to the phase separation of the saturated glycerol–water domains and the excess water that eventually arranges into growing ice crystals.[60]

We also note that under the present experimental conditions, we are limited to the smallest size of the crystallites we can resolve in the order of 10 nm. Below this, the peaks become very broad and comparable to the background.[63] Thus, we cannot exclude that the nanocrystals nucleate already during the cooling, although no ice Bragg peaks are observed (see Figure 2A).

In Figure 3 (top row), we present the temperature dependence of the SAXS $I(Q)$ peak position Q_m^{SAXS} as a function of temperature. Interestingly, as seen in panel A, the interference peak at ≈ 1 nm^{-1} at room temperature in the SAXS $I(Q)$s corresponding to the protein–protein interactions shows different trends depending on whether the sample is being cooled (blue) or heated (red). Furthermore, the magnitude of the observed hysteresis depends on the final quench temperature. Starting from room temperature, the peak gradually shifts toward lower Q values until $T \approx 245 \pm 1$ K. When cooling past this temperature, the slope increases significantly. Upon reheating the sample, however, the temperature dependence in Figure 3 exhibits a different path, corresponding to lower Q_m^{SAXS} values for the same temperature. On the other hand, for the shallow quench shown in Figure 3C, i.e., for $T_{quench} = 245$ K, the hysteresis is reduced.

The bottom row in Figure 3 shows the temperature dependencies of the WAXS $I(Q)$ peak position Q_m^{WAXS}. Note that the WAXS data were measured simultaneously with the SAXS curves, i.e., during the same temperature cycles discussed above for the SAXS data. Similarly, when the sample is cooled down to $T = 195$ K, a crossover in the temperature dependence of the peak position is observed at $T \approx 245$ K (Figure 3D) with a significant hysteresis upon the full temperature sweep. The hysteresis becomes less apparent for the middle quench down to $T = 225$ K (Figure 3E) and disappears completely for the shallow quench to $T = 245$ K (Figure 3F). We note that similar thermal hysteresis in the protein structure factor has been observed before[6] and attributed to the formation of ice in hydration water for moderately hydrated protein powders.

To elucidate the changes occurring in the system during the temperature variation, we study the protein–protein structure factor, $S(Q)$, extracted from the fits of the SAXS data (Figure 1B). The obtained structure factor captures a pronounced shift of the low-Q peak toward lower Q values upon cooling observed in the experimental SAXS $I(Q)$ shown in Figure 1B. The temperature evolution of the structure factor upon cooling the sample from room temperature down to $T = 195$ K is shown in Figure 4A. The TY-potential parameters used are fixed to $Z_1 = 21$, $Z_2 = 3.5$, and $K_2 = 3.2 k_B T$, and the interparticle attraction parameter K_1 is the fitting parameter. The K_1 variation in the whole temperature range (blue for cooling, red for warming up) and the resulting TY-potentials at each temperature are plotted in panels B and C, respectively.
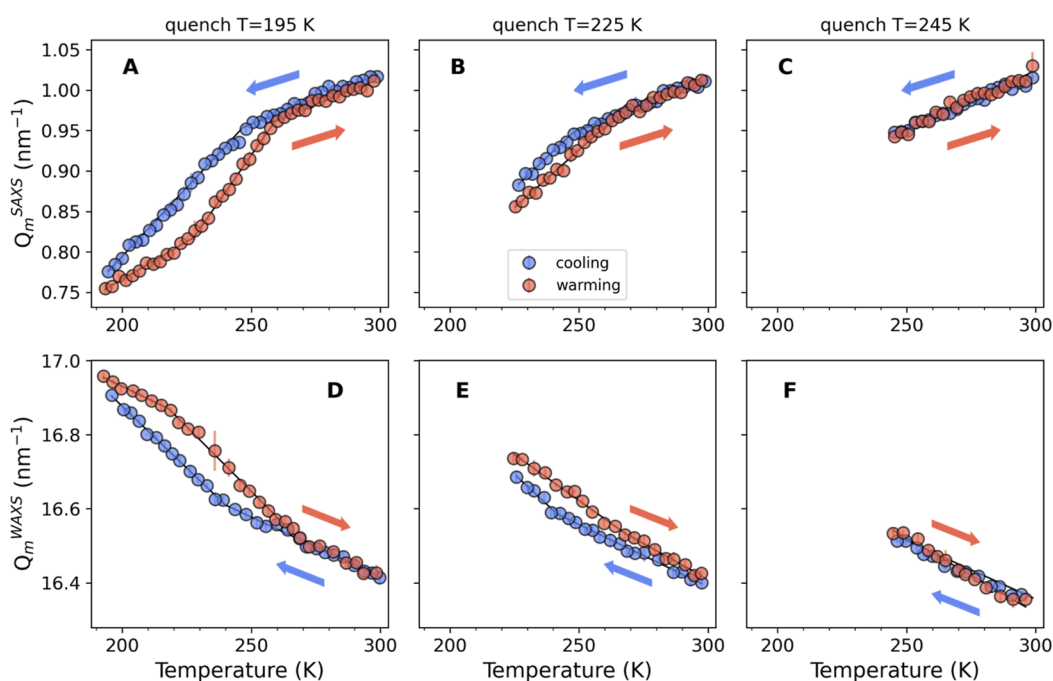
Figure 3. Top row: temperature dependence of the Q-value of the SAXS $I(Q)$ peak position for a 200 mg/mL lysozyme in glycerol−water solution during different temperature cycles: (A) deep quench with T_{quench} = 195 K, (B) medium quench with T_{quench} = 225 K, and (C) shallow quench with T_{quench} = 245 K. Bottom row: the temperature dependence of Q-value of WAXS $I(Q)$ peak position during different temperature cycles: (D) deep, (E) medium, and (F) shallow quench, simultaneously measured for the same sample. The colors indicate measurements performed upon cooling (blue) or warming (red), as shown by the arrows.
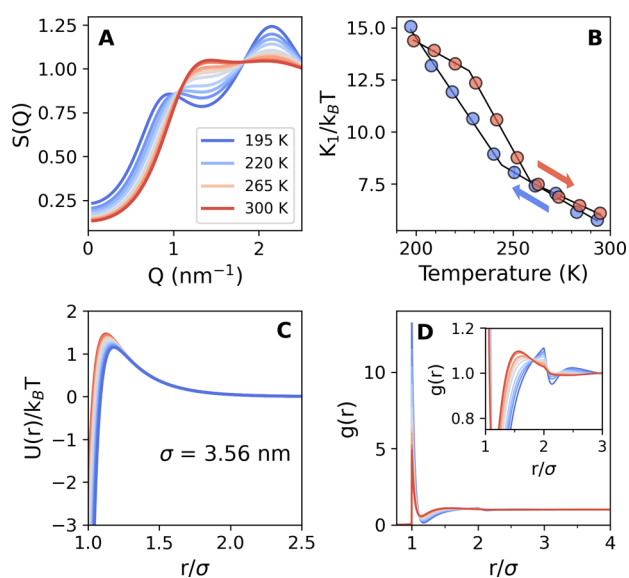

Figure 4. (A) Protein−protein structure factor $S(Q)$ obtained from the fits using the two-Yukawa (TY) model shown in Figure 1B at different temperatures upon cooling. (B) Temperature dependence of the attraction strength parameter K_1 extracted from fitting the SAXS curves upon cooling down (blue) and warming up (red). The other TY parameters were fixed to Z_1 = 21, Z_2 = 3.5, and K_2 = 3.2$k_B T$. (C) Temperature evolution of TY potential upon cooling down. (D) The pair distribution function $g(r)$ derived from the modeled structure factors shown in (A). The inset shows details of the $g(r)$ second coordination shell.

In agreement with the previous studies on lysozyme solutions under ambient conditions,[38,40] the effective attraction increases upon cooling for the entire temperature range probed here. Furthermore, the temperature dependence of the K_1

parameter exhibits a crossover at $T \approx$ 245 K upon cooling, i.e., at a similar temperature where the crossovers in the experimental $I(Q)$s are observed (see Figure 3A,D). Also, here we present, shown in red, the extracted K_1 parameter from the fits of the SAXS data acquired during heating. Intuitively, the hysteresis shape resembles that obtained from the analysis of the peak in SAXS plotted in Figure 3A.

To further elucidate the physical mechanism responsible for the observed changes of the protein−protein interaction at low temperatures, we calculate the pair distribution function, $g(r)$, from the corresponding structure factor at different temperatures. The value of $g(r)$ describes the probability of finding another particle at a distance r from the reference particle. Shown in Figure 4D is the variation of $g(r)$ upon cooling from room temperature down to 195 K. For all temperatures, when $r/\sigma < 1$, $g(r) = 0$, consistent with the shape of the potential in panel C. The peak at $r/\sigma = 1$ indicates the probability to find particles contact pairs owing to high protein concentration in the studied system.

Upon cooling, the intensity of the first maximum at $r/\sigma \approx 1$ corresponding to the first coordination shell rises sharply, resulting in a depletion in the range between $r/\sigma \approx 1.1$ and $r/\sigma \approx 1.2$. The latter also suggests that the interstitial protein molecules between the first and second coordination shell rearrange toward a more regular structure. Consistent with the observed increase in the attraction strength, the tendency for a higher probability density of first-neighbors is expected at lower temperatures. Furthermore, the second coordination maximum located at $r/\sigma \approx 1.5$ at room temperature gradually shifts toward larger distances with decreasing temperature. Eventually, at temperatures below 245 K, a pronounced feature in the $g(r)$ is developed at $r/\sigma \approx 2$, characteristic of finding an in-line configuration of three touching particles.[41,43] Overall, the observed behavior of the pair distribution function suggests
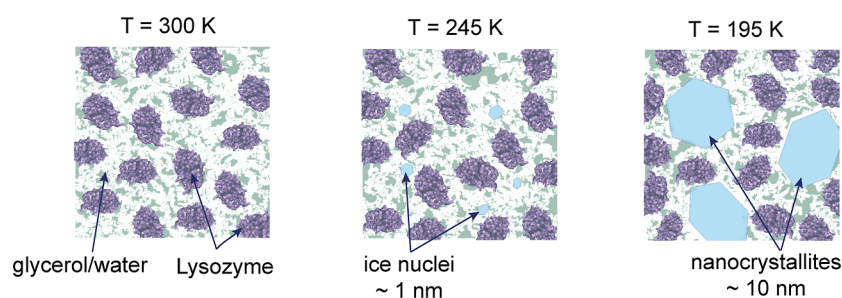
Figure 5. Schematic illustration of the changes occurring in the lysozyme solution in the glycerol—water mixture upon cooling below the melting point of the solvent (245 K), where ice crystallites start to nucleate, down to 195 K, where the nanocrystallites evolve further and grow upon reheating.

an enhancement of the ordered arrangement of the protein molecules in the intermediate range upon cooling.

Assuming the observed crossover upon cooling below $\approx$245 K occurs due to ice nanocrystallite formation (Figure 5), it can be deduced that the glycerol concentration in the remaining solvent slightly changes due to the expelled glycerol from the ice.[28,29,60] As a result, the protein—protein interactions below this temperature occur in an effectively different environment at colder temperatures. This interpretation is consistent with the observed increase of the slope of the attraction strength K_1 after the crossover temperature, which can be related to the decrease of the dielectric permittivity of the medium.[31]

Furthermore, during the formation of the ice crystallites, the structure of the solvation layer, i.e., the layer around the protein, is expected to change as well. Previous studies suggest that in aqueous solutions, as the glycerol concentration increases above 50 vol %, glycerol molecules are more included into the protein solvation shell,[20] which otherwise is highly disfavored from the vicinity of the protein.[34,55] In turn, the composition of the surface layer can affect the protein—protein interactions,[64] which in our case manifests in the kink in the observed temperature dependence of the attraction strength K_1. Consequently, the restructuring is reflected in the changes in the pair distribution function and the position of the correlation peak in SAXS.

CONCLUSIONS

In conclusion, we present a simultaneous SAXS/WAXS study of the lysozyme solution in glycerol—water mixture in a broad temperature range from room temperature to $\approx$195 K. We follow the temperature evolution of the protein—protein peak in SAXS as well as the interatomic structure peak in WAXS upon cooling down and heating. The hysteresis observed in both SAXS and WAXS upon the full temperature cycle is attributed to the formation of nanocrystallites with the size of $\approx$10 nm, which are evident by the Bragg peaks in the WAXS during heating. Furthermore, the observed crossover at 245 K upon cooling is found both in SAXS and WAXS, which coincides with the melting temperature of the solution. We attribute this effect to the ice nuclei formation occurring already upon cooling down below the melting point of the solutions.

Since we do not observe any significant temperature-dependent changes in the protein radius of gyration R_g, we tentatively conclude that this transition does not reflect cold denaturation. Instead, we attribute this transition to changes in the protein—protein interaction potential stemming from the

influence of the solvent due to the nanocrystals, which is modeled by the two-Yukawa potential. The model indicates that this effect is reflected in the protein—protein structure factor peak and results in increased protein—protein attraction. From the observed variation of the pair distribution function, we infer that upon cooling the interstitial range in the probability density between first and second protein—protein coordination shell is depleted due to the increased attraction term between the lysozyme molecules.

Our results shed light on the influence of nanocrystallites on protein—protein interactions and the functional mechanisms of cryoprotectants at low temperatures. These insights can advance our understanding of protein stability in supercooled environments, with important implications for biotechnical cryostorage applications and for the development of new technologies and materials to improve our ability to survive and thrive in cold and icy environments.

ASSOCIATED CONTENT

Data Availability Statement

The data that support the findings of this study are openly available in the figshare repository with DOI: https://su.figshare.com/articles/dataset/Nanocrystallites_Modulate_Intermolecular_Interactions_in_Cryoprotected_Protein_Solutions/23295626}{10.17045/sthlmuni.23295626.

ⓢ Supporting Information

The Supporting Information is available free of charge at https://pubs.acs.org/doi/10.1021/acs.jpcb.3c02413.

Measurement protocol, radiation damage assessment, measurement of WAXS intensity, temperature dependence of the Q-value of WAXS $I(Q)$ peak position for the 10 mg/mL lysozyme solution in glycerol-water mixture and pure solvent, and representative 2D scattering patterns in the WAXS range (PDF)

AUTHOR INFORMATION

Corresponding Authors

Mariia Filianina − *Department of Physics, AlbaNova University Center, Stockholm University, S-106 91 Stockholm, Sweden;* ⓞ orcid.org/0000-0002-1366-7360; Email: mariia.filianina@fysik.su.se

Fivos Perakis − *Department of Physics, AlbaNova University Center, Stockholm University, S-106 91 Stockholm, Sweden;* ⓞ orcid.org/0000-0001-9863-9811; Email: f.perakis@fysik.su.se

Authors

Maddalena Bin − *Department of Physics, AlbaNova University Center, Stockholm University, S-106 91 Stockholm, Sweden;* ⦿ orcid.org/0000-0003-4906-9335

Sharon Berkowicz − *Department of Physics, AlbaNova University Center, Stockholm University, S-106 91 Stockholm, Sweden*

Mario Reiser − *Department of Physics, AlbaNova University Center, Stockholm University, S-106 91 Stockholm, Sweden;* ⦿ orcid.org/0000-0003-0160-9478

Hailong Li − *Department of Physics, AlbaNova University Center, Stockholm University, S-106 91 Stockholm, Sweden; Max Plank Institute for Polymer Research, 55128 Mainz, Germany*

Sonja Timmermann − *Department of Physics, Universität Siegen, 57072 Siegen, Germany;* ⦿ orcid.org/0000-0002-5428-9044

Malte Blankenburg − *Deutsches Elektronen-Synchrotron (DESY), 22607 Hamburg, Germany*

Katrin Amann-Winkel − *Department of Physics, AlbaNova University Center, Stockholm University, S-106 91 Stockholm, Sweden; Max Plank Institute for Polymer Research, 55128 Mainz, Germany; Institute of Physics, Johannes Gutenberg University, 55128 Mainz, Germany;* ⦿ orcid.org/0000-0002-7319-7807

Christian Gutt − *Department of Physics, Universität Siegen, 57072 Siegen, Germany*

Complete contact information is available at:
https://pubs.acs.org/10.1021/acs.jpcb.3c02413

Notes

The authors declare no competing financial interest.

■ REFERENCES

(1) Storey, K. B.; Storey, J. M. Freeze tolerance in animals. *Physiol. Rev.* **1988**, *68*, 27−84.

(2) Hubálek, Z. Protectants used in the cryopreservation of microorganisms. *Cryobiology* **2003**, *46*, 205−229.

(3) Doster, W.; Cusack, S.; Petry, W. Dynamical transition of myoglobin revealed by inelastic neutron scattering. *Nature* **1989**, *337*, 754−756.

(4) Ringe, D.; Petsko, G. A. The 'glass transition' in protein dynamics: what it is, why it occurs, and how to exploit it. *Biophys. Chem.* **2003**, *105*, 667−680.

(5) Doster, W.; Busch, S.; Gaspar, A. M.; Appavou, M.-S.; Wuttke, J.; Scheer, H. Dynamical transition of protein-hydration water. *Phys. Rev. Lett.* **2010**, *104*, 098101.

(6) Fitter, J. The temperature dependence of internal molecular motions in hydrated and dry alpha-amylase: the role of hydration water in the dynamical transition of proteins. *Biophys. J.* **1999**, *76*, 1034−1042.

(7) Chen, S.-H.; Liu, L.; Fratini, E.; Baglioni, P.; Faraone, A.; Mamontov, E. Observation of fragile-to-strong dynamic crossover in protein hydration water. *Proc. Natl. Acad. Sci. U.S.A.* **2006**, *103*, 9012−9016.

(8) Cordone, L.; Ferrand, M.; Vitrano, E.; Zaccai, G. Harmonic behavior of trehalose-coated carbon-monoxy-myoglobin at high temperature. *Biophys. J.* **1999**, *76*, 1043−1047.

(9) Paciaroni, A.; Cinelli, S.; Onori, G. Effect of the environment on the protein dynamical transition: A neutron scattering study. *Biophys. J.* **2002**, *83*, 1157−1164.

(10) Tsai, A. M.; Neumann, D. A.; Bell, L. N. Molecular dynamics of solid-state lysozyme as affected by glycerol and water: a neutron scattering study. *Biophys. J.* **2000**, *79*, 2728−2732.

(11) Caliskan, G.; Kisliuk, A.; Sokolov, A. P. Dynamic transition in lysozyme: role of a solvent. *J. Non-Cryst. Solids* **2002**, *307−310*, 868−873.

(12) Fenimore, P. W.; Frauenfelder, H.; Magazù, S.; McMahon, B. H.; Mezei, F.; Migliardo, F.; Young, R. D.; Stroe, I. Concepts and problems in protein dynamics. *Chem. Phys.* **2013**, *424*, 2−6.

(13) Frauenfelder, H.; Chen, G.; Berendzen, J.; Fenimore, P. W.; Jansson, H.; McMahon, B. H.; Stroe, I. R.; Swenson, J.; Young, R. D. A unified model of protein dynamics. *Proc. Natl. Acad. Sci. U.S.A.* **2009**, *106*, 5129−5134.

(14) Fenimore, P.; Frauenfelder, H.; McMahon, B.; Young, R. Bulk-solvent and hydration-shell fluctuations, similar to α- and β-fluctuations in glasses, control protein motions and functions. *Proc. Natl. Acad. Sci. U.S.A.* **2004**, *101*, 14408−14413.

(15) Caliskan, G.; Kisliuk, A.; Tsai, A. M.; Soles, C. L.; Sokolov, A. P. Protein dynamics in viscous solvents. *J. Chem. Phys.* **2003**, *118*, 4230−4236.

(16) Caliskan, G.; Mechtani, D.; Roh, J. H.; Kisliuk, A.; Sokolov, A. P.; Azzam, S.; Cicerone, M. T.; Lin-Gibson, S.; Peral, I. Protein and solvent dynamics: How strongly are they coupled? *J. Chem. Phys.* **2004**, *121*, 1978−1983.

(17) Ronsin, O.; Caroli, C.; Baumberger, T. Preferential hydration fully controls the renaturation dynamics of collagen in water-glycerol solvents. *Eur. Phys. J. E: Soft Matter Biol. Phys.* **2017**, *40*, 55.

(18) Jansson, H.; Bergman, R.; Swenson, J. Role of solvent for the dynamics and the glass transition of proteins. *J. Phys. Chem. B* **2011**, *115*, 4099−4109.

(19) Dirama, T. E.; Carri, G. A.; Sokolov, A. P. Coupling between lysozyme and glycerol dynamics: Microscopic insights from molecular-dynamics simulations. *J. Chem. Phys.* **2005**, *122*, 244910.

(20) Hirai, M.; Ajito, S.; Sugiyama, M.; Iwase, H.; Takata, S.-I.; Shimizu, N.; Igarashi, N.; Martel, A.; Porcar, L. Direct evidence for the effect of glycerol on protein hydration and thermal structural transition. *Biophys. J.* **2018**, *115*, 748.

(21) Tanaka, H. Liquid−liquid transition and polyamorphism. *J. Chem. Phys.* **2020**, *153*, 130901.

(22) Murata, K.-I.; Tanaka, H. Liquid−liquid transition without macroscopic phase separation in a water−glycerol mixture. *Nat. Mater.* **2012**, *11*, 436−443.

(23) Farnum, M.; Zukoski, C. Effect of glycerol on the interactions and solubility of bovine pancreatic trypsin inhibitor. *Biophys. J.* **1999**, *76*, 2716−2726.

(24) Daschakraborty, S. How do glycerol and dimethyl sulphoxide affect local tetrahedral structure of water around a nonpolar solute at low temperature? Importance of preferential interaction. *J. Chem. Phys.* **2018**, *148*, 134501.

(25) Murata, K.-I.; Tanaka, H. General nature of liquid−liquid transition in aqueous organic solutions. *Nat. Commun.* **2013**, *4*, 2844.

(26) Bachler, J.; Fuentes-Landete, V.; Jahn, D. A.; Wong, J.; Giovambattista, N.; Loerting, T. Glass polymorphism in glycerol—water mixtures: II. Experimental studies. *Phys. Chem. Chem. Phys.* **2016**, *18*, 11058−11068.

(27) Bachler, J.; Handle, P. H.; Giovambattista, N.; Loerting, T. Glass polymorphism and liquid—liquid phase transition in aqueous solutions: experiments and computer simulations. *Phys. Chem. Chem. Phys.* **2019**, *21*, 23238−23268.

(28) Hayashi, Y.; Puzenko, A.; Balin, I.; Ryabov, Y. E.; Feldman, Y. Relaxation dynamics in glycerol-water mixtures. 2. Mesoscopic feature in water rich mixtures. *J. Phys. Chem. B* **2005**, *109*, 9174−9177.

(29) Hayashi, Y.; Puzenko, A.; Feldman, Y. Ice nanocrystals in glycerol-water mixtures. *J. Phys. Chem. B* **2005**, *109*, 16979−16981.

(30) Yoshimura, Y.; Ishikawa, Y.; Takekiyo, T. Cryopreservation of proteins in aqueous DMSO solutions at cryogenic temperature: A case study of lysozyme. *J. Mol. Liq.* **2019**, *273*, 663−669.

(31) Javid, N.; Vogtt, K.; Krywka, C.; Tolan, M.; Winter, R. Protein—protein interactions in complex cosolvent solutions. *ChemPhysChem* **2007**, *8*, 679−689.

(32) Esposito, A.; Comez, L.; Cinelli, S.; Scarponi, F.; Onori, G. Influence of glycerol on the structure and thermal stability of lysozyme: A dynamic light scattering and circular dichroism study. *J. Phys. Chem. B* **2009**, *113*, 16420−16424.

(33) Bonincontro, A.; Risuleo, G. Dielectric spectroscopy as a probe for the investigation of conformational properties of proteins. *Spectrochim. Acta, Part A* **2003**, *59*, 2677−2684.

(34) Sinibaldi, R.; Ortore, M. G.; Spinozzi, F.; Carsughi, F.; Frielinghaus, H.; Cinelli, S.; Onori, G.; Mariani, P. Preferential hydration of lysozyme in water/glycerol mixtures: A small-angle neutron scattering study. *J. Chem. Phys.* **2007**, *126*, 235101.

(35) Venkataramani, S.; Truntzer, J.; Coleman, D. R. Thermal stability of high concentration lysozyme across varying pH: A Fourier Transform Infrared study. *J. Pharm. BioAllied Sci.* **2013**, *5*, 148.

(36) Pfeil, W.; Privalov, P. L. Thermodynamic investigations of proteins: III. Thermodynamic description of lysozyme. *Biophys. Chem.* **1976**, *4*, 41−50.

(37) Ashiotis, G.; Deschildre, A.; Nawaz, Z.; Wright, J. P.; Karkoulis, D.; Picca, F. E.; Kieffer, J. The fast azimuthal integration Python library: pyFAI. *J. Appl. Crystallogr.* **2015**, *48*, 510−519.

(38) Shukla, A.; Mylonas, E.; Di Cola, E.; Finet, S.; Timmins, P.; Narayanan, T.; Svergun, D. I. Absence of equilibrium cluster phase in concentrated lysozyme solutions. *Proc. Natl. Acad. Sci. U.S.A.* **2008**, *105*, 5075−5080.

(39) Liu, Y.; Chen, W.-R.; Chen, S.-H. Cluster formation in two-Yukawa fluids. *J. Chem. Phys.* **2005**, *122*, 044507.

(40) Möller, J.; Schroer, M. A.; Erlkamp, M.; Grobelny, S.; Paulus, M.; Tiemeyer, S.; Wirkert, F. J.; Tolan, M.; Winter, R. The effect of ionic strength, temperature, and pressure on the interaction potential of dense protein solutions: from nonlinear pressure response to protein crystallization. *Biophys. J.* **2012**, *102*, 2641−2648.

(41) Liu, Y.; Porcar, L.; Chen, J.; Chen, W.-R.; Falus, P.; Faraone, A.; Fratini, E.; Hong, K.; Baglioni, P. Lysozyme protein solution with an intermediate range order structure. *J. Phys. Chem. B* **2011**, *115*, 7238−7247.

(42) Biehl, R. Jscatter, a program for evaluation and analysis of experimental data. *PLoS One* **2019**, *14*, No. e0218789.

(43) Riest, J.; Nägele, G.; Liu, Y.; Wagner, N. J.; Godfrin, P. D. Short-time dynamics of lysozyme solutions with competing short-range attraction and long-range repulsion: Experiment and theory. *J. Chem. Phys.* **2018**, *148*, 065101.

(44) Kim, S. B.; Palmer, J. C.; Debenedetti, P. G. Computational investigation of cold denaturation in the Trp-cage miniprotein. *Proc. Natl. Acad. Sci. U.S.A.* **2016**, *113*, 8991−8996.

(45) Kozuch, D. J.; Stillinger, F. H.; Debenedetti, P. G. Low temperature protein refolding suggested by molecular simulation. *J. Chem. Phys.* **2019**, *151*, 185101.

(46) Cardinaux, F.; Stradner, A.; Schurtenberger, P.; Sciortino, F.; Zaccarelli, E. Modeling equilibrium clusters in lysozyme solutions. *Europhys. Lett.* **2007**, *77*, 48004.

(47) Joshi, K.; Bhuyan, A. K. Quasi-native transition and self-diffusion of proteins in water-glycerol mixture. *Biophys. Chem.* **2020**, *257*, 106274.

(48) Graziano, G. On the mechanism of cold denaturation. *Phys. Chem. Chem. Phys.* **2014**, *16*, 21755−21767.

(49) Arsiccio, A.; McCarty, J.; Pisano, R.; Shea, J.-E. Heightened cold-denaturation of proteins at the ice—water interface. *J. Am. Chem. Soc.* **2020**, *142*, 5722−5730.

(50) Strambini, G.; Gabellieri, E. Proteins in frozen solutions: evidence of ice-induced partial unfolding. *Biophys. J.* **1996**, *70*, 971−976.

(51) Fink, A. L.; Angelides, K. J. Papain-catalyzed reactions at subzero temperatures. *Biochemistry* **1976**, *15*, 5287−5293.

(52) Travers, F.; Douzou, P. Dielectric constant of mixed solvents used for a low temperature biochemistry. *Biochimie* **1974**, *56*, 509−514.

(53) Akerlof, G. Dielectric constants of some organic solvent-water mixtures at various temperatures. *J. Am. Chem. Soc.* **1932**, *54*, 4125−4139.

(54) Pohl, F. M. Kinetics of reversible denaturation of trypsin in water and water—ethanol mixtures. *Eur. J. Biochem.* **1968**, *7*, 146−152.

(55) Gekko, K.; Timasheff, S. N. Mechanism of protein stabilization by glycerol: preferential hydration in glycerol-water mixtures. *Biochemistry* **1981**, *20*, 4667−4676.

(56) Timasheff, S. N. The control of protein stability and association by weak interactions with water: how do solvents affect these processes? *Annu. Rev. Biophys. Biomol. Struct.* **1993**, *22*, 67−97.

(57) Fink, A. L. Cryoenzymology: The use of sub-zero temperatures and fluid solutions in the study of enzyme mechanisms. *J. Theor. Biol.* **1976**, *61*, 419−445.

(58) Stradner, A.; Sedgwick, H.; Cardinaux, F.; Poon, W. C. K.; Egelhaaf, S. U.; Schurtenberger, P. Equilibrium cluster formation in concentrated protein solutions and colloids. *Nature* **2004**, *432*, 492−495.

(59) Chen, Z.; Huang, C.; Yao, X.; Benmore, C. J.; Yu, L. Structures of glass-forming liquids by x-ray scattering: Glycerol, xylitol, and D-sorbitol. *J. Chem. Phys.* **2021**, *155*, 244508.

(60) Popov, I.; Greenbaum Gutina, A.; Sokolov, A. P.; Feldman, Y. The puzzling first-order phase transition in water—glycerol mixtures. *Phys. Chem. Chem. Phys.* **2015**, *17*, 18063−18071.

(61) Langford, J. I.; Wilson, A. J. C. Scherrer after sixty years: A survey and some new results in the determination of crystallite size. *J. Appl. Crystallogr.* **1978**, *11*, 102−113.

(62) Moreau, D. W.; Atakisi, H.; Thorne, R. E. Ice in biomolecular cryocrystallography. *Acta Crystallogr., Sect. D: Struct. Biol.* **2021**, *77*, 540−554.

(63) Sellberg, J. A.; Huang, C.; McQueen, T. A.; Loh, N. D.; Laksmono, H.; Schlesinger, D.; Sierra, R. G.; Nordlund, D.; Hampton, C. Y.; Starodub, D.; et al. Ultrafast X-ray probing of water structure below the homogeneous ice nucleation temperature. *Nature* **2014**, *510*, 381−384.

(64) Shulgin, I. L.; Ruckenstein, E. Various contributions to the osmotic second virial coefficient in protein-water-cosolvent solutions. *J. Phys. Chem. B* **2008**, *112*, 14665−14671.